

Progress in Nuclear Energy  
Manuscript Draft

Manuscript Number: PNUCENE-D-16-00455

Title: Analysis the effects of error in movement of control rods for a WWER-1000 Nuclear Reactor by developed external coupling system

Article Type: Research Paper

Keywords: WWER-1000, Monte Carlo method, single heated channel model, pin power calculation, point kinetic model

1

2

3

4

5                   **Analysis the effects of error in movement of control rods for a WWER-1000 Nuclear**  
6                   **Reactor by developed external coupling system**

7                   **Reza Akbari<sup>\*</sup>, Dariush Rezaei, Ahmad Gharib**

8  
9                   Amirkabir University of Technology (Tehran Polytechnic), Department of Energy

10  
11                   Engineering & Physics, Tehran, Iran.

12

13

14

15

16

17

18

19

20

21

22

23

24

25

26

27

28

29

30

31

32

33

34

35

36

37

38

39

40

41

42

43

44

45

46

47

48

49

50

51

52

53

54

55

56

57

58

---

59                   <sup>\*</sup> Corresponding author.  
60                   E-mail address: [Reza\\_Akbari@aut.ac.ir](mailto:Reza_Akbari@aut.ac.ir) (Reza Akbari).

61

62

63

64

65

## ABSTRACT

Error in movement of control rods that leads to Error in suppression of xenon oscillations refer to anticipated operational occurrences. Errors related to this occurrence could be treated as a long-term absence of some special actions used to stabilize the power field or incorrect movements of the control and protection system absorber rod. In this study, the movement of control rod, causing maximum power tilt, has been simulated in a WWER-1000 reactor by using coupling system contains Monte Carlo method for neutronic calculations, a single heated channel model for thermal hydraulic calculations and point kinetic model that all of these components are externally coupled by MATLAB system. The results of developed single heated channel model have been checked with RELAP5 results for WWER-1000. Analyses are based on linear heat rate of the most-powered fuel rod according to the WWER-1000 final safety analysis report. First, we determined the position of this most-powered fuel rod at desired cycle time steps by our developed coupling system. Then the most-powered fuel rod is segmented axially into equally spaced zones to study the effect of axial linear heat rate profile during desired transient. Finally, the results have been compared with Final Safety Analysis Report of WWER-1000 reactor. It is seen that there is a proper similarity between calculated and reported results.

**Keywords:** WWER-1000, Monte Carlo method, single heated channel model, pin power calculation, point kinetic model.

### 1. Introduction

Power distribution is controlled by movement of the selected groups of the control and protection system absorber rods (CPS AR) In accordance with the assigned algorithm on the basis of continuous monitoring of the core power using the in-core instrumentation system.

1 The reactor operator has special procedures to control the axial power distribution using  
2 control mechanisms (such as full- and part-length control rods) to minimize the effects of  
3 xenon redistribution and axial power redistribution during load-follow operations.  
4  
5

6 Transients of xenon distributions that lead to power spatial oscillations are known as xenon  
7 oscillations. In cores of WWER-1000 type reactors, xenon oscillations are usually defined as  
8 the self-sustaining redistribution of iodine and xenon that may occur during the core power  
9 loading.

10  
11  
12  
13  
14  
15  
16 Indeed in large reactors, the phenomenon of xenon instability can occur when reactor  
17 operating at high thermal neutron flux levels at which the rate of xenon burnout is important  
18 relative to the rate of xenon decay. This phrase refers to the process, thereby causing a change  
19 in power density, whether on a local or global basis, perturbs the xenon distribution and the  
20 thermal neutron absorption cross section oscillations in the core.  
21  
22  
23  
24  
25  
26  
27

28 Xenon oscillation has been studied by both numerical simulations and experiments since the  
29 introduction of reactors (Ansarifar et al., 2015; Parhizkari et al., 2015; Hosseini et al., 2015;  
30 Reiss et al., 2011; Marseguerra et al., 2003), but in this study we want to focus on effects of  
31 these oscillations on important local power changes of reactor core not xenon concentration.  
32  
33  
34  
35  
36  
37

38 The power oscillations arising from xenon are not a nuclear hazard; because there isn't any  
39 reason for reactor core to become supercritical. The main problem is local increasing in  
40 neutron flux. It means that fission heat is generated more rapidly than is expected. Thus,  
41 there is a possibility of fuel damage resulting from an excess power density. For this reason,  
42 minimizing axial peak of local power densities during reactor operation, while maintaining  
43 the necessary load change flexibility is a very important safety aspect of nuclear reactor plant  
44 control.  
45  
46  
47  
48  
49  
50  
51  
52  
53  
54

55 In this research, we used MATLAB software to develop a coupling system. In this coupling  
56 system MCNPX as a Monte Carlo method code has been used for neutronic calculations,  
57  
58  
59  
60  
61  
62  
63  
64  
65

Not clear

? PE

QED

OBJECTIVE  
(?)  
NOT CLEAR !

NJOY code has been used to feed cross section in desired temperatures to the MCNPX code and a single heated channel model has been used for thermal hydraulic calculations. Also during control rod movement point kinetic model has been used as interface between neutronic and thermal-hydraulic methods. The movement of control rod causing maximum possible power field tilt has been simulated according to the operator's error in suppression of xenon oscillations scenario available on Bushehr Nuclear Power Plant Final Safety Analysis Report (FSAR). Noori-Kalkhoran et al. (2016 and 2014) used WIMSD-5B, PARCS V2.7 and COBRA-EN, Vahman et al. (2016) used a set of RELAP5/ WIMSD/ PARCS codes and also Elsawi et al. (2015) used WIMS9/PARCS/TRACE codes to simulate the reactor transient behavior in our coupling system. Because the need for pin power calculations more accurate, MCNPX as a Monte Carlo method has been used. Pirouzmand and Roosta (2016) recently used MCNPX for WWER-1000 burnup calculations, but here we used this code linked with thermal-hydraulic and kinetic models for evaluation of a dynamic process.

## 2. Simulation tools

### 2.1 MCNPX 2.7

In this study, BNPP reactor core model is simulated by MCNPX 2.7 code and NJOY. Monte Carlo method is based on simulating individual particles and recording some aspects of their behaviors. The Monte Carlo N-Particle MCNP code is a continuous energy time dependent transport code. The MCNPX 2.7 is general-purpose, continuous-energy, generalized geometry, burnup calculation capability, and various particle transport calculation code.

In this method the results are based on the history of each particle so the solution derived is more accurate and no approximations are performed. This is because the results are based on the history of each particle. This makes the Monte Carlo-based code MCNP as an ideal method and hence a computational tool of choice to develop an exact reference solution (Briemeister, 2013). MCNP code is used in many studies for neutronic analysis (Galahom et

Not clear  
WHAT ARE  
THEIR  
CONTRIBUTION  
TO THE  
FIELD?

PE

⇒ NOT REALLY DESCRIPTIONS OF EITHER MCNP & NJOY!  
WHAT ARE THE FUNDAMENTALS FOR BOTH MODELS? WHY  
ARE THEY USED FOR? ARE THERE ANY CONSTRAINTS IN THESE MODELS?  
ARE THESE MODELS TESTED & RELEVANT FOR YOUR CALCULATIONS?  
al., 2015; Ivanov et al., 2013). In this study, we used NJOY code for producing cross section

1 data library in various temperatures.  
2  
3  
4

## 2.2 NJOY

7 The NJOY nuclear data processing system is a comprehensive computer code package for  
8 producing pointwise and multigroup cross sections and related quantities from evaluated  
9 nuclear data in the ENDF format. NJOY is a modular computer code used for converting  
10 evaluated nuclear data in the ENDF format into different types of libraries useful for  
11 applications calculations. The NJOY code can be used for simulation neutrons, photons, and  
12 charged particles transitions problems, and it can produce libraries for a wide variety of  
13 particle transport and reactor analysis codes (MacFarlane, 2000).

24 The ACER module in NJOY code prepares libraries in the ACE format (A Compact ENDF)  
25 for the MCNP continuous-energy Monte Carlo code. The ACE format contains all the details  
26 of the normal ENDF format but the representation of the data is different for the sake of  
27 efficiency. So, by using of NJOY code we can produce ACE format cross section libraries at  
28 the desired temperatures that can be used directly in MCNP calculations.

## 3.3 Single Heated Channel Model

38 Temperature profile calculations of fuel assemblies and fuel rod channels in desired time step  
39 of fuel burnup have a very important role in finding the location of hot rod and hot channel  
40 and also accuracy of final results. For this purpose, we used single heated channel model that  
41 is fast and also relatively accurate (Todreas and Kazimi, 1993). Single heated channel model  
42 is a one dimensional heat conduction/convection model that is used for each channel. The  
43 hydraulic calculations of this model is based on the laws of conservations of mass (Eq. (1)),  
44 momentum (Eq. (2)), and energy (Eq. (3)).

$$\frac{\partial \rho}{\partial t} + \nabla \cdot (\rho \vec{v}) = 0 \quad (1)$$

$$\frac{\partial}{\partial t} \rho \vec{v} + \nabla \cdot (\rho \vec{v} \vec{v}) = \nabla p + \nabla \cdot \vec{f} \quad (2)$$

$$\frac{\partial}{\partial t} \rho h + \nabla \cdot (\rho h \vec{v}) = -\nabla \cdot \dot{q}'' + \dot{q}''' + \frac{\partial p}{\partial t} + \nabla \cdot (p \vec{v}) + \bar{\tau} : \nabla \vec{v} \quad (3)$$

In single heated channel model for single phase and steady state condition, fluid pressure, enthalpy and temperature along the length of each channel, finally will be attained from Eqs.

(4-6).

$$P_{in} - P_{out} = \left( \frac{G_m^2}{\rho_m^+} \right)_{out} - \left( \frac{G_m^2}{\rho_m^+} \right)_{in} + \int_{z_{in}}^{z_{out}} \frac{f G_m |G_m|}{2 D_e \rho_m} dz + \int_{z_{in}}^{z_{out}} g \rho_m dz \quad (4)$$

$$dh_m = \left[ \frac{q'' P_h}{\dot{m}} + \frac{1}{\rho_m} \left( \frac{\partial p}{\partial z} + \frac{f G_m |G_m|}{2 D_e \rho_m} \right) \right] dz \quad (5)$$

$$T(z) = \frac{1}{C_p} \int_{z_{in}}^z \left[ \frac{q'' P_h}{\dot{m}} + \frac{1}{\rho_m} \left( \frac{\partial p}{\partial z} + \frac{f G_m |G_m|}{2 D_e \rho_m} \right) \right] dz + T_{in} \quad (6)$$

For convective heat transfer coefficient calculation we used Dittus-Boelter correlation (Todreas and Kazimi, 1993). According to the heat convective and conduction equations, for calculation of the outer and inner temperature of clad and the outer temperature of fuel, Eqs. (7-9) have been used.

$$T_{co}^z = \frac{q'(z)}{2 \pi R_{co}^{hot} h_{cool}} + T_{cool}(z) \quad (7)$$

$$T_{ci}(z) = q^\circ(z) \frac{1}{2 \pi k_c} \ln \frac{R_{co}^{hot}}{R_{ci}^{hot}} + T_{co}(z) \quad (8)$$

$$T_{Fo}(z) = \frac{q''}{h_g} + T_{ci}(z) \quad (9)$$

m: ?  
 $G_m$ : ?  
 $z$ : ? } WHERE  
 DID THESE  
 EQNS.  
 COME FROM?

Where  
 DID THESE  
 EQNS.  
 COME  
 FROM?

the gap conductance of the fuel-clad gap that is shown in Eq. (10) which in this equation  
 conductance of the gap is the sum of heat transfer across the open gap and heat transfer  
 coefficient for gap closure (occurs because of fuel swelling and thermal expansion). PE?

$$h_g = h_{g,open} + h_{g,closure} \quad (10)$$

The heat transfer coefficient for open gap is obtained: flow

$$h_{g,open} = \frac{k_{gas}}{\delta_{eff}} + \frac{\sigma}{\frac{1}{\epsilon_f} + \frac{1}{\epsilon_c} - 1} \frac{T_{Fo}^4 - T_{Fi}^4}{T_{Fo} - T_{Fi}} \quad \leftarrow \text{THIS EQN DOESN'T LOOK CORRECT!} \quad (11)$$

According to Eq. (12) effective gap width can be calculated where  $\delta_g$  is gap width and  $\delta_{jump}$   
 is found to be 10 mm (Todreas and Kazimi, 1993).

$$\delta_{eff} = \delta_g + \delta_{jump}$$

The gas conductivity of a pure gas is given by Eq. (13), where A is 15.8 and T is the gas  
 temperature.

$$k(\text{pure gas}) = A \times 10^{-6} T^{0.79} \quad W/cm \quad (13)$$

According to the Calza-Bini calculations, the closure heat transfer coefficient is given by Eq.  
 (14) (Calza-Bini et al. 1975), where  $p_i$  is surface contact pressure and for zircaloy cladding,  
 Meyer's hardness number (H) is  $14 \times 10^4$ .

$$h_{closure} = c \frac{2k_f k_c}{k_f + k_c} \frac{p_i}{H \sqrt{\delta_g}} \quad (14)$$

Finally the inner fuel temperature can be obtained as follows:

$$T_f^{in} = T_f^{out} + \frac{\dot{q}'' R_{fo}^2}{4k_f} \left\{ 1 - \left( \frac{R_{fi}}{R_{fo}} \right)^2 \left( 1 + \ln \left( \frac{R_{fo}}{R_{fi}} \right)^2 \right) \right\} \quad (15)$$

$\bar{\kappa}_f : ?$

The flowchart of developed model for T-H calculation that is used to calculate fuel, clad and coolant temperatures for each channel is shown in Fig. 1.

## 2.4 Reactor kinetics analysis

In order to analyze the transient response of a reactor to both normal operating conditions and postulated accident situations, one must utilize the nuclear reactor kinetics equations. Reactor kinetics analysis plays an important role in core design, since it is necessary to assess safety margins, to select and place control and safety instrumentation, to design the control and protective systems, and to determine the need and effectiveness of engineered safeguards. At our coupling system, a numerical solution of the reactor kinetics equations describing the neutron flux time behavior in the core has been used. In this study, we used point kinetics equation to treat time behavior of power.

The point kinetics equations are shown in Eqs. (16) and (17) (Henry, 1975):

$$\frac{dP(t)}{dt} = \frac{\rho(t) - \bar{\beta}(t)}{\Lambda(t)} P(t) + \sum_{i=1}^{N_c} \lambda_i \bar{C}_i(t) \quad (16)$$

$$\begin{array}{c} \bar{\beta} \\ \Lambda \\ \bar{C}_i \\ \lambda_i \end{array} \quad ? \quad (17)$$

$$\frac{\partial \bar{C}_i(t)}{\partial t} = \frac{\bar{\beta}_i(t)}{\Lambda(t)} P(t) - \lambda_i \bar{C}_i(t) \quad (17)$$

In this study we used Runge Kutta fourth order numerical method (Eq. (18)) for solving Eqs. (16) and (17):

$$P_{i+1} = P_i + \frac{\Delta t}{6} (k_1 + 2k_2 + 2k_3 + k_4) \quad (18)$$

$k ?$

## 2. Description of Bushehr NPP

1 Bushehr NPP is one of the WWER-1000 (V-446) reactors that has a hexagonal configuration  
2 and 1/6 symmetric shape. This reactor has 163 hexagonal fuel assemblies of the same  
3 geometry and producing 3000 MWth at full power (AEOI, 2003). Moreover, each fuel  
4 assembly contains 311 fuel rods and 18 guiding channels for control rods or burnable  
5 poisons. Bushehr NPP full core model is given in Fig. 2. Some specifications of Bushehr NPP  
6 that used in this simulation are given in Table 1. Also all banks of reactor control cluster  
7 assemblies are shown in Fig. 3. According to the FSAR in full power normal operation of  
8 reactor, only 10% of bank number 10 is inserted in the core and all of other banks are out the  
9 core.

#### 21 4. Operator's error in suppression of xenon oscillations scenario

22 For simulating Operator's error in suppression of xenon oscillations in Bushehr NPP, we used  
23 the scenario that introduced in Bushehr NPP FSAR. This scenario is shown in Table 2.

24 According to the BNPP FSAR, The given conditions are accompanied with more severe  
25 consequences than under the reactor start-up from the hot standby mode, because in the  
26 course of their scenario the requirements for the reactor operation at intermediate constant  
27 power levels are not met. According to the BNPP FSAR this scenario is applied for two  
28 different periods, one in the BOC and another for EOC. In the initial state of transient for  
29 both BOC and EOC periods 25% of CPS AR group number 10 is placed on the core. In the  
30 final state after transient calculation related to the CPS movement for both BOC and EOC  
31 periods, all of CPS AR group number 10 is placed completely out of core (AEOI, 2003).

#### 32 5. Simulation

33 Initially for surveying the thermal-hydraulic model accuracy, the single heated channel model  
34 has been checked for WWER-1000 reactor core as a typical single heated with presented  
35 specifications in Table 1.

Then the single heated channel results are compared to RELAP5 code (RELAP5 code development Team, 1995). Figs. 4-6 show the profile of temperature and pressure of fluid and temperature of clad respectively. These figures show that the single heated channel has relatively proper results.

PE For finding core materials (coolant, clad and fuel) temperature profile in desired time step of cycle burnup, we used a coupling between single heated channel model, NJOY and MCNPX in MATLAB system. The flowchart of this coupling during steady state and burnup calculation is presented in Fig. 7. According to this flowchart we can attain core desired parameters in desired time step of burnup cycle.

Then NJOY code is used to generate cross section libraries for each material that exist in the core at desired temperatures.

In this calculation, BNPP reactor core model is designed and developed by MCNPX code. This model contains all physical core components that are used in real reactor operating conditions. In this study, as shown in Fig. 8, the reactor core geometry which is modeled in MCNPX, covers all fuel rods (fuel, gap and clad), guide channels, burnable absorber rods, control rods, baffle, and barrel.

The geometry is modeled in a way that we can replace rod cluster control assemblies in desired position. Furthermore by using of the BURN card, burnup effect with axial variation in the core is modeled. For more accuracy, simulations are carried out with high number of histories.

Since the MCNPX results are normalized to one source neutron, the result has to be properly scaled in order to get absolute comparison of the measured quantities such as flux, reaction rate, fission density, etc. The F4 tally results can be scaled to a desired power level. The scaling factor can be introduced on the FM (tally multiplier) card or can be used later in data processing. After some calculation the power density equation has been derived as Eq. (19):

Except FIG 4,  $T_{c,0}$  &  $P$  for both method do NOT match! Why?

CONFUSION

?

$$p(r) = P\bar{v}N \int_0^{20\text{Mev}} \sigma_f(E)\varphi_{F4}(E) dE \quad (19)$$

P denotes reactor nominal power,  $\bar{v}$  denotes the average number of neutrons released per fission, N denotes fissile material atom density,  $\sigma_f$  microscopic total fission cross section and  $\varphi_{F4}$  denotes flux attained from MCNPX tally F4 output. Eq. (19) can be applied in MCNPX as below:

F4:N (Cell number)

FM4 (-3.0E+09 1 (-6 -7))

$P=3.0\text{E}+09$  Watt, 1 denotes fissile material number in MCNP, -6 (in MCNPX) $\equiv \bar{v}$ , -7 (in MCNPX) $\equiv \sigma_f$ .

The easiest way for calculating the power density distribution can be done by using the superimposed mesh tally card, FMESHn. FMESH card allows the user to define a mesh tally superimposed over the problem geometry. The FMESH card is extremely powerful and useful method also for calculating power peaking factors. By using the very fine mesh we can calculate local power peaking and power density distributions near the guide channels, which are very difficult if not impossible to do with deterministic methods.

In our simulation we used two different coupling procedures for burnup calculation during steady state condition (Fig. 7) and another for transient condition. The flowchart of coupling procedure during transient that developed in MATLAB system is presented in Fig. 9. It's obvious that the position of most powered fuel pin will change after control rod movement, so to survey the hot pin rod, this position is determined again for our calculations.

For surveying xenon oscillation same as BNPP FSAR, we considered linear heat rate in most powered fuel rod. Linear heat rate is defined as Eqs. (20-22).

$$Q_l = q_l \times K_0 \times K_{eng} \times K_n \quad (20)$$

$$K_0 = K_r \times K_z \quad (21)$$

$$K_r = K_q \times K_k \quad (22)$$

Which the values and parameters in these equations defined according to the BNPP FSAR as below:

$q_1$ : Average linear heat rate (166.7 W/cm), defined as a ratio of the nominal thermal power to the total length of fuel in all fuel rods at the operating mode;

$K_0$ : Linear heat rate peaking factor, defined as a ratio of the maximum linear heat rate of the fuel rod to the average value in the core with nominal technological parameters of fuel;

$K_r$ : Fuel rod power peaking factor, defined as a ratio of the maximum fuel rod power to the average value in the core;

$K_{eng}$ : Engineering safety factor for local heat flux;

$K_n$ : Coefficient of accounting for uncertainty of reactor thermal power determination and maintenance (1.04);

$K_z$ : Ratio of linear heat rate in fuel rod to the average value of heat rate for the given fuel rod:

$K_q$ : Power peaking factor for FAs in the core;

$K_k$ : Power peaking factor for fuel rod in FA.

## 6. Results

The reactor core geometry which is modeled in MCNPX is shown in Fig. 8. First, in the steady state condition to confirm the input data and evaluate precision of codes and parameters; calculations of the radial power peaking factor (PPF) in the beginning of cycle (BOC) and end of cycle (EOC), with xenon equilibrium poisoning in the situation that 10% of control rod bank 10 (CPS control group) is in the active core, have been done by our coupling system and compared with FSAR's results. Figs. 10 and 11 show a comparison between values of radial PPF for xenon equilibrium poisoning in the BOC and EOC respectively. Relative differences were predicted according to the below equation:

IN THESE FIGS, the "RELATIVE ERROR",  
ARE THEY IN %?

Relative Differences =  $\left| \frac{\text{PPF}_{\text{FSAR}} - \text{PPF}_{\text{MCNPX}}}{\text{PPF}_{\text{FSAR}}} \right| \times 100$  (23)

As seen in Figs. 10 and 11, the PPF values in the BOC and EOC from MCNPX output show a great similarity to the FSAR values.

In this study, analyses are based on linear heat rate of the most-powered fuel rod in the BOC and EOC. So first, we must determine the position of this most-powered fuel rod in the BOC and EOC separately. Figs. 12 and 13 show values of Fuel rod power peaking factor ( $K_r$ ) in the fuel assembly that most-powered fuel rod placed for the BOC and EOC respectively.

After the determination of the most-powered fuel rod for the BOC and EOC, the most-powered fuel rod is divided into equally spaced zones in axial direction to study the effect of axial linear heat rate profile. Figs. 14 and 15 show axial linear heat rate profile in steady state condition for the BOC and EOC respectively.

The most unfavourable positions and ranges of CPS AR control group movement are considered with account for their allowable control range. According to the BNPP FSAR for initial condition, 25% of control rod bank 10 is in the active core. Figs. 16 and 17 show axial linear heat rate profile in initial condition for the BOC and EOC respectively.

In particular, during burnup the lowest position of CPS AR working group is simulated to obtain the results in the most unfavourable axial power distribution. Figs. 18 and 19 represent the distributions of axial linear heat rate of the most-powered fuel rods (final condition) for the BOC and EOC respectively after the transient calculations. It should be noted that the given conditions are referred to the category of anticipated operational occurrences and in the course of their scenario; the realization of linear heat rate values is possible.

The reactivity changes due to this scenario are extremely slow and allow the operator or the control system to detect and compensate the changes. Normally, these operating reactivity changes can be handled by the automatic control system, which would insert or withdraw

control rod assemblies to maintain the correct power level and thus limit the reactor coolant system temperature change.

## 7. Conclusion

In this study, the movement of control rod causing maximum possible power field tilt has been simulated in a WWER-1000 reactor by using coupling system contain NJOY and MCNPX codes, single heated channel model and point kinetic model. The ability of NJOY code in producing cross section library for MCNPX in desired temperatures that attained from single heated channel model and furthermore the ability of coupling procedure for CPS movement available in our coupling system helped us to determine the axial linear heat rate profile and position of most-powered fuel rod at a desired time step. The results attained from our coupling system have a proper match with data available in FSAR. It must be mentioned that although the results are proper, but using the Monte Carlo method in our coupling system was computationally too expensive but here we focused on accuracy of results. According to the results, the power oscillations arising from xenon are not a nuclear hazard, in the sense that there is a danger that the reactor will become supercritical. The main problem is that a local increase in the neutron flux means that fission heat is generated more rapidly than is expected. In WWER-1000 with reliable monitoring of power distribution, occurrence of significant errors in suppression of xenon oscillations is unlikely and of short-term nature, but in case of errors during suppression of xenon oscillations, safety criteria are met.

## Reference

Ansarifar, G. R., Esteki, M. H., Arghand, M., 2015. Sliding mode observer design for a PWR to estimate the xenon concentration & delayed neutrons precursor density based on the two point nuclear reactor model. Prog. Nucl. Energy 79, 104-114.

Atomic energy organization of Iran (AEOI), 2003. Final Safety Analysis Report (FSAR) for Bushehr WWER-1000 reactor, Tehran, Iran.

- Briemeister, J.F., 2013. MCNPX a General Monte Carlo N-particle Transport Code, Version X.2.7. Los Alamos National Laboratory. La-13709.
- Calza-Bini, A., Cosoli, G., Filacchioni, G., Lanchi, M., Nobili, A., Pesce, E., Rocca, U., Rotoloni, P.L., 1975. In-pile measurement of fuel cladding conductance for pelleted and vipac zircaloy-2 sheathed fuel pin. Nucl. Technol. 25, 103.
- Elsawi, M.A., Bin Hraiz,A.S., 2015. Benchmarking of the WIMS9/PARCS/TRACE code system for neutronic calculations of the Westinghouse AP1000™ reactor. Nucl. Eng. Des. 293, 249–257.
- Galahom, A. A., Bashter, I. I., Aziz, M., 2015. Neutronic analysis and validation of boiling water reactor core designed by MCNPX code. Ann. Nucl. Energy 76, 461-468.
- Henry, A.F., 1975. Nuclear Reactor Analysis. MIT Press, Cambridge, Massachusetts.
- Hosseini, M., Khalafi, H., Khakshournia, S., 2015. Two group, three dimensional diffusion theory coupled with single heated channel model: A study based on xenon transient simulation of Tehran research reactor. Prog. Nucl. Energy 85, 108-120.
- Ivanov, A., Sanchez, V., Stieglitz, R., Ivanov, K., 2013. High fidelity simulation of conventional and innovative LWR with the coupled Monte-Carlo thermal-hydraulic system MCNP-SUBCHANFLOW. Nucl. Eng. Des. 262, 264–275.
- MacFarlane, R.E., 2000. NJOY-99. Nuclear Data Processing System.  
[<http://t2.lanl.gov/codes/njoy99/index.html>](http://t2.lanl.gov/codes/njoy99/index.html).
- Marseguerra, M., Zio, E., Torri, G., 2003. Power density axial oscillations induced by xenon dynamics:Parameter identification via Genetic algorithms. Prog. Nucl. Energy 43, 365-372.
- Noori-Kalkhoran, O., Minuchehr, A., Shirani, A.S., Rahgoshay, M., 2014. Full scope thermal-neutronic analysis of LOFA in a WWER-1000 reactor core by coupling PARCS v2.7 and COBRA-EN. Prog. Nucl. Energy 74, 193-200.
- Noori-Kalkhoran, O., Yarizadeh-Beneh, M., Ahangari, R., 2016. Development of external coupling for calculation of the control rod worth in terms of burn-up for a WWER-1000 nuclear reactor. Nucl. Eng. Des. 305, 612–625.
- Parhizkari, H., Aghaie, M., Zolfaghari, A., Minuchehr, A., 2015. An approach to stability analysis of spatial xenon oscillations in WWER-1000 reactors. Ann. Nucl. Energy 79, 125-132.

1 Pirouzmand, A., Roosta, F., 2016. Calculation of radial burnup and nuclides atom density  
2 distributions in a VVER-1000 fuel rod using Monte Carlo method. Prog. Nucl. Energy 88,  
3 321-331.  
4

5  
6 Reiss, T., Fehér, S., Czifrus, Sz, 2011. Xenon oscillation in SCWRs. Prog. Nucl. Energy 53,  
7 457-462.  
8

9  
10 RELAP5 code development Team, 1995. RELAP5/MOD3 Code Manual, Idaho National  
11 Engineering Laboratory.  
12

13  
14 Todreas, N.E., Kazimi, M.S., 1993. Nuclear System, Thermal Hydraulic Fundamentals,  
15 Hemisphere Publishing Corporation, New York.  
16

17  
18 Vahman, N., Akbari-Jeyhouni, R., Rezaei Ochbelagh, D., Amrollahi, R., 2016. An  
19 assessment of a VVER-1000 core during Turbo-Generator load reduction test using  
20 RELAP5/MOD3.2 and WIMSD-5B/PARCSv2.7. Prog. Nucl. Energy 93, 155-164.  
21  
22  
23  
24  
25  
26  
27  
28  
29  
30  
31  
32  
33  
34  
35  
36  
37  
38  
39  
40  
41  
42  
43  
44  
45  
46  
47  
48  
49  
50  
51  
52  
53  
54  
55  
56  
57  
58  
59  
60  
61  
62  
63  
64  
65

## Appendix 1. Nomenclature.

1	$A_z$	<i>Cross sectional area of the channel;</i>
2	$C_p$	<i>Specific heat of the fluid;</i>
3	$D_e$	<i>Hydraulic diameter;</i>
4	$f$	<i>Friction factor;</i>
5	$f_b$	<i>Body force;</i>
6	$g$	<i>Gravity;</i>
7	$h$	<i>Enthalpy;</i>
8	$h_{cool}$	<i>Nusselt number;</i>
9	$h_{g,closure}$	<i>Heat transfer coefficient for gap closure;</i>
10	$h_{g,open}$	<i>Heat transfer across the open gap;</i>
11	$k_f$	<i>Thermal conductivity coefficient of the fuel;</i>
12	$k_{gas}$	<i>Thermal conductivity of the gas;</i>
13	$p$	<i>Pressure;</i>
14	$(p_h)$	<i>Heated perimeter;</i>
15	$\dot{q}'$	<i>Linear heat source;</i>
16	$\dot{q}''$	<i>Wall heat flux;</i>
17	$\dot{q}'''$	<i>Volumetric heat source;</i>
18	$R_{ci}$	<i>Clad inner radius;</i>
19	$R_{co}$	<i>Clad outer radius;</i>
20	$R_{fi}$	<i>Inner radius of fuel;</i>
21	$R_{fo}$	<i>Outer radius of fuel;</i>
22	$T_{ci}$	<i>Inner temperature of clad;</i>
23	$T_{co}$	<i>Outer temperature of clad;</i>
24	$T_{fi}$	<i>Inner fuel temperature;</i>
25	$T_{fo}$	<i>Outer fuel temperature;</i>
26	<b>Greek letters</b>	
27	$\delta_{eff}$	<i>Effective gap width;</i>
28	$\varepsilon_c$	<i>Surface emissivity of the clad;</i>
29	$\varepsilon_f$	<i>Surface emissivity of the fuel;</i>
30	$\sigma$	<i>StefaneBoltzmann constant;</i>
31	$\vec{v}$	<i>Coolant velocity;</i>
32	$\rho$	<i>Coolant density; and</i>
33	$\tau$	<i>Shear stress.</i>

1  
2  
3  
4  
5  
6  
7  
8  
9  
10  
11  
12  
13  
14  
15  
16  
17  
18  
19  
20  
21  
22  
23  
24  
25  
26  
27  
28  
29  
30  
31  
32  
33  
34  
35  
36  
37  
38  
39  
40  
41  
42  
43  
44  
45  
46  
47  
48  
49  
50  
51  
52  
53  
54  
55  
56  
57  
58  
59  
60  
61  
62  
63  
64  
65

1  
2  
3  
4  
**Table 1**5  
6  
7 Bushehr NPP reactor core specifications.  
8  
9  
10  
11  
12  
13  
14  
15  
16  
17  
18  
19  
20  
21  
22  
23  
24  
25  
26  
27  
28  
29  
30  
31  
32  
33  
34  
35  
36  
37  
38  
39  
40  
41  
42  
43  
44  
45  
46  
47  
48  
49  
50  
51  
52  
53  
54  
55  
56  
57  
58  
59  
60  
61  
62  
63  
64  
65

Parameter	Value
Maximum heat power of reactor, 104% of nominal power (MW)	3120
Fraction of coolant leaks bypassing the core (%)	4.0
Coolant pressure at the core outlet (MPa)	$15.7 \pm 0.3$
Coolant temperature at the reactor inlet ( $^{\circ}$ C)	$291 \pm 2.5$
Average coolant temperature at the reactor outlet ( $^{\circ}$ C)	$321 \pm 5.0$
Average linear heat rate (W/cm)	166.0
Maximum linear heat rate (W/cm)	448
Steam generator steam capacity (t/h)	1470
Fuel assembly form	Hexagonal
Arrangement of fuel rod	Triangle
Number of fuel assembly in the core	163
Fuel assembly pitch (mm)	236
Fuel rod pitch (mm)	12.75
Number of fuel rods in the FA (Pcs)	311
Hole diameter in the fuel pellet (mm)	1.5
Fuel pellet outside diameter (mm)	7.57
Cladding outside diameter (mm)	9.1
Cladding material	Alloy Zr + 1% Nb
Fuel pellet material	UO <sub>2</sub>
Fuel mass in the rod (kg)	1.575
Fuel rod effective height (cm)	353
Number of control rod	$85 \times 18$
Control rod absorbing material	B <sub>4</sub> C + (Dy <sub>2</sub> O <sub>3</sub> - TiO <sub>2</sub> )
Number of burnable poison rod per bundle (Pcs)	18

1  
2      **Table 2**  
3  
4

5      The sequence of events for calculation of axial linear heat rate.  
6  
7  
8  
9  
10  
11  
12  
13  
14  
15  
16  
17  
18  
19  
20  
21  
22  
23  
24  
25  
26  
27  
28  
29  
30  
31  
32  
33  
34  
35  
36  
37  
38  
39  
40  
41  
42  
43  
44  
45  
46  
47  
48  
49  
50  
51  
52  
53  
54  
55  
56  
57  
58  
59  
60  
61  
62  
63  
64  
65

Sequence of events	State
1	Steady state: operation at nominal parameters.
2	Initial state: partially immersed working group of CPS AR keep the unsteady axial offset at the upper limit of permissible values.
3	Erroneous movement or complete withdrawal of CPS AR working group from the core: tilt of axial power field occurs that could result in exceeding the limitations on linear heat flux.
4	During normal operation and with the availability of monitoring, control and diagnostics system, the preventive protection signal will actuate in order to prohibit the working group withdrawal and for power decrease to a safe level without violating the limits established for critical parameters.

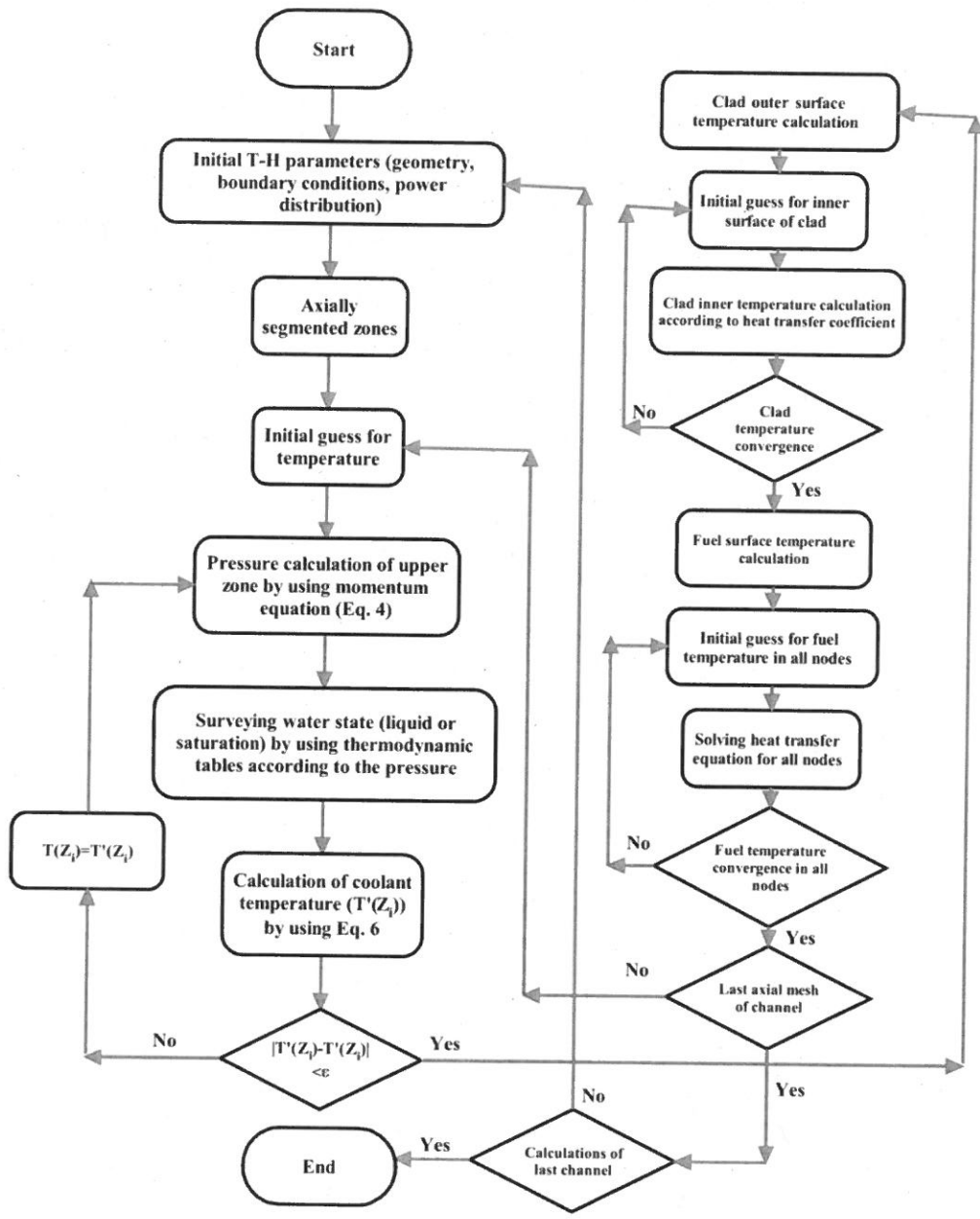


**Fig. 1.** The flowchart of developed single heated channel model.

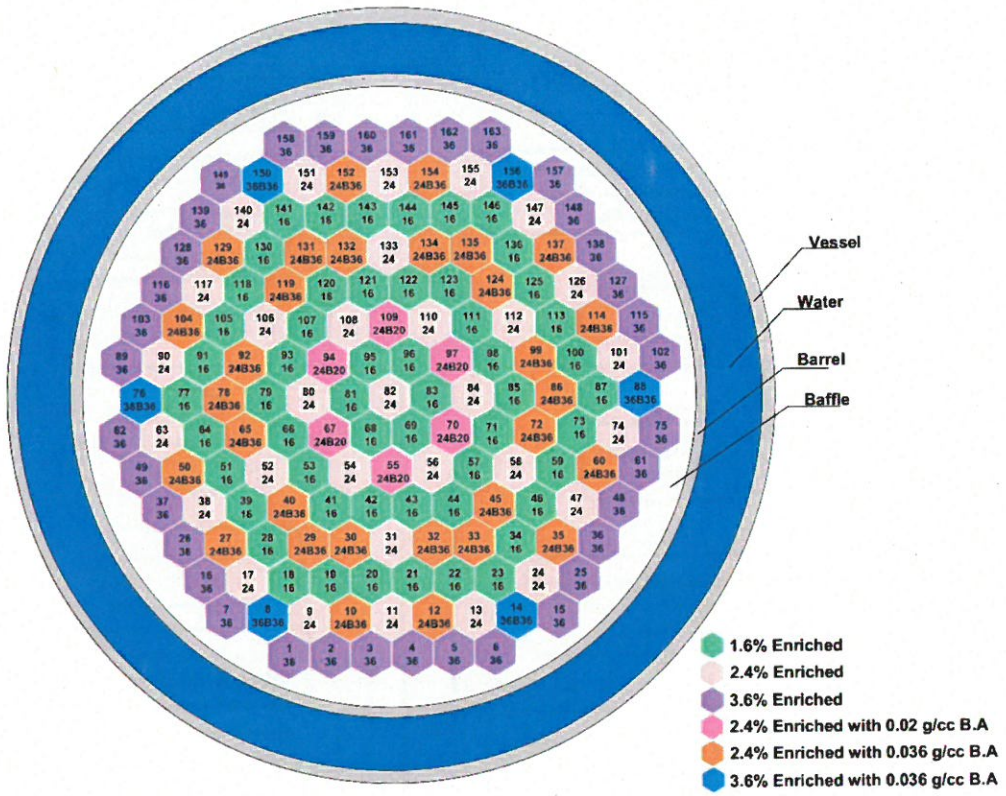


Fig. 2. Bushehr NPP reactor core arrangement.



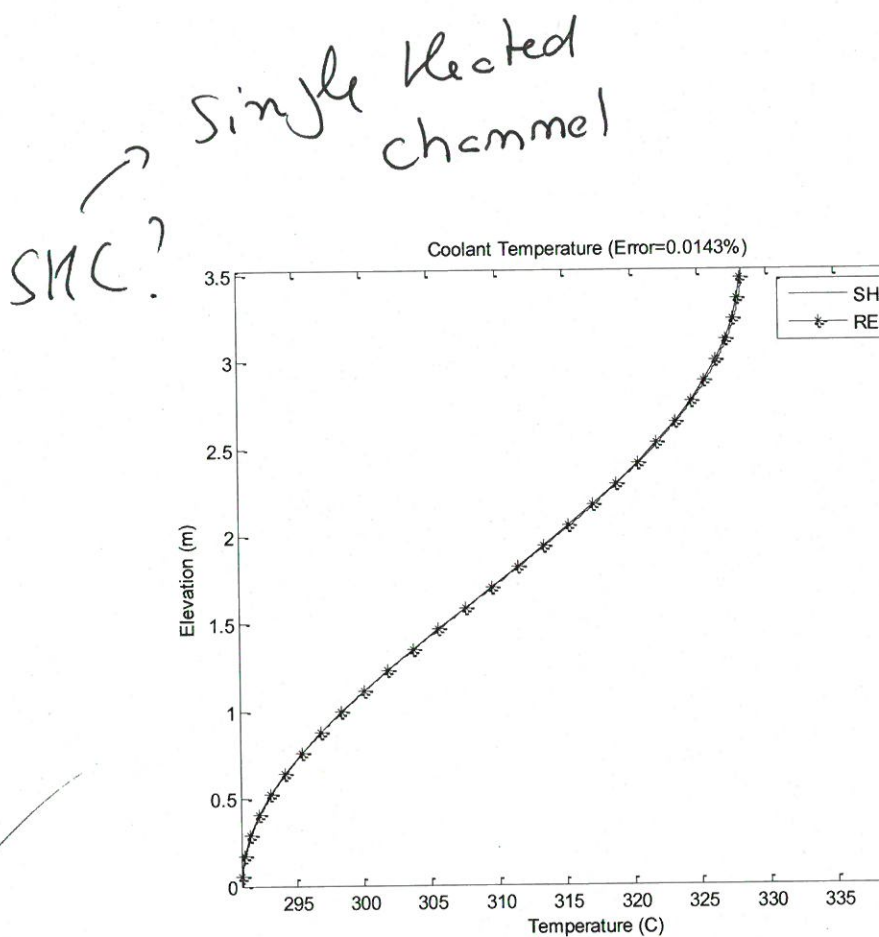


Fig. 4. Temperature profile of coolant.

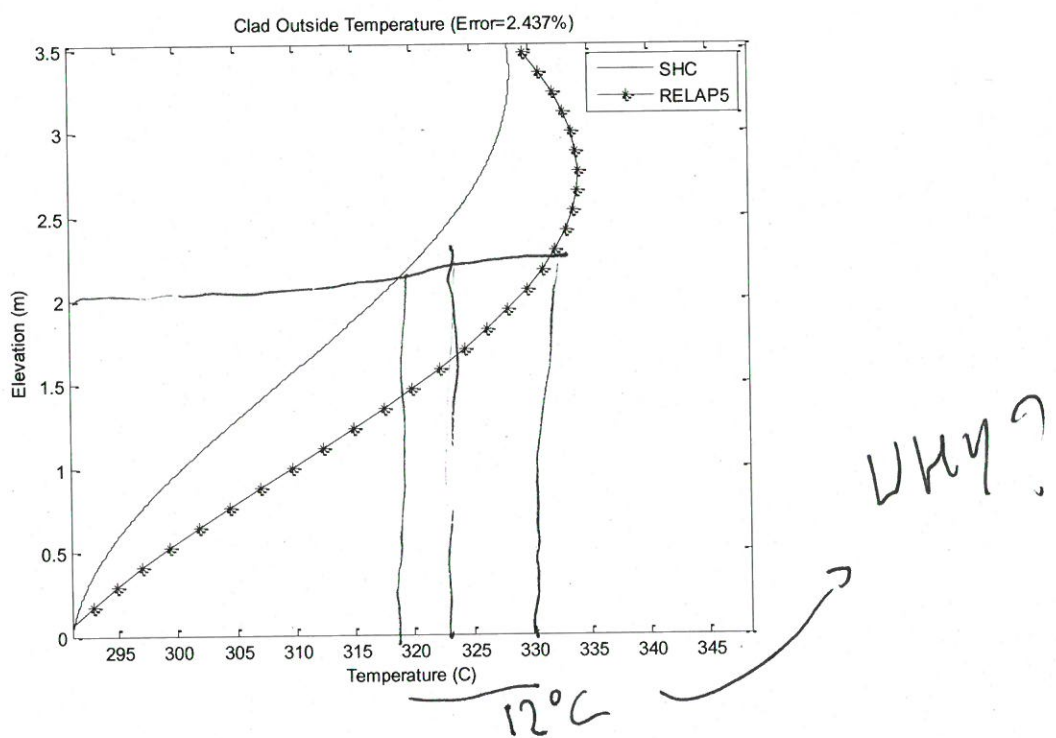
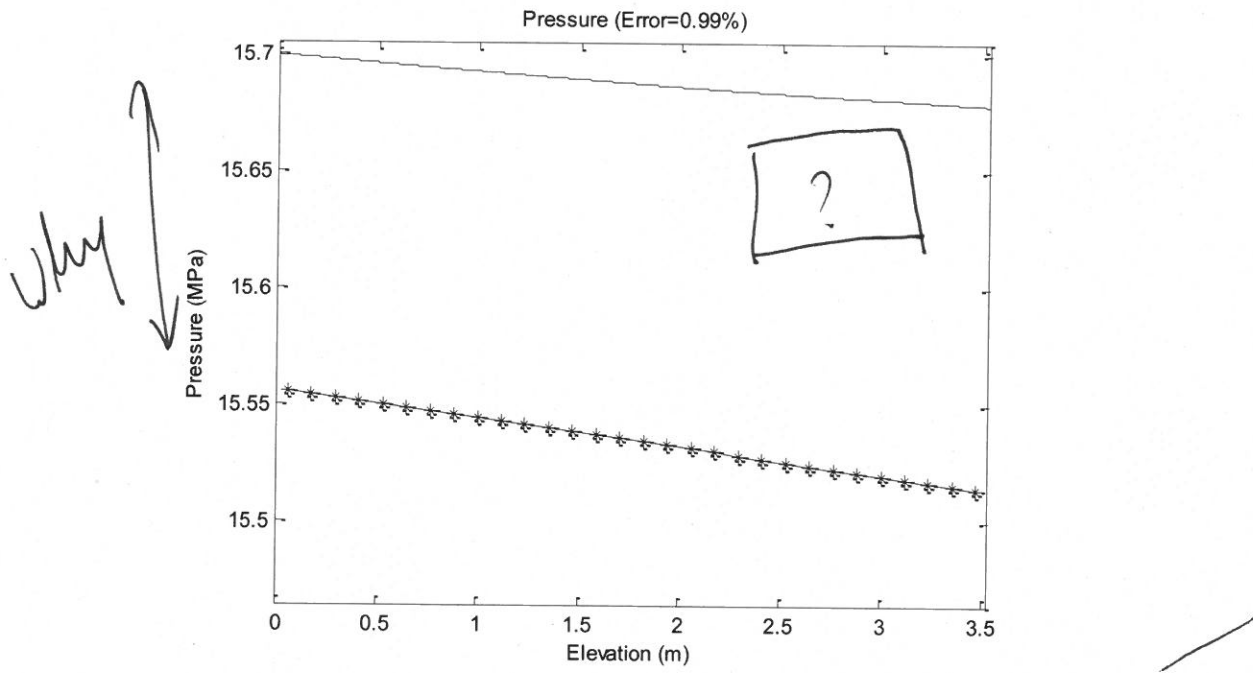


Fig. 5. Temperature profile of clad outside.

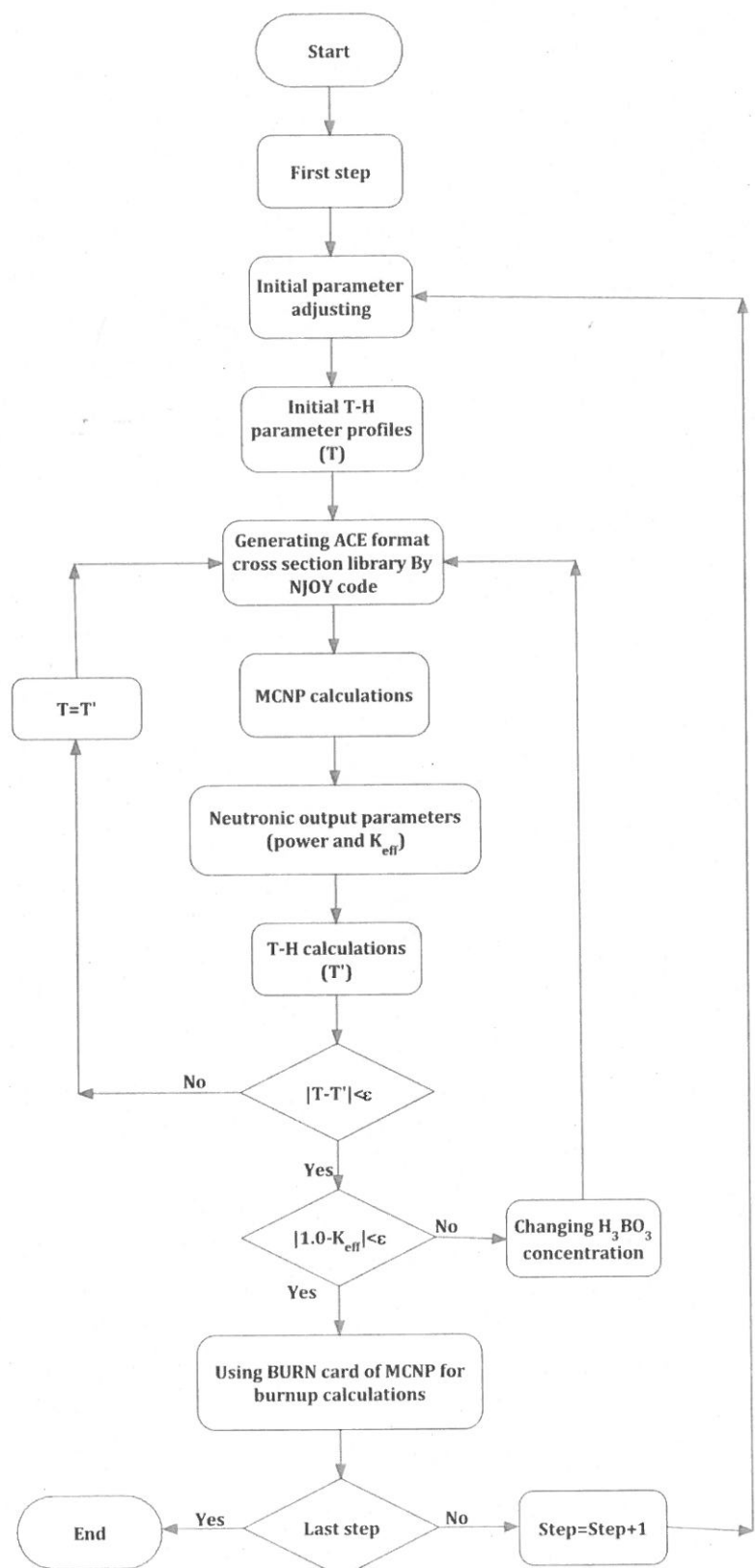
1  
2  
3  
4  
5  
6  
7  
8  
9

10  
11  
12  
13  
14  
15  
16  
17  
18  
19  
20  
21  
22  
23  
24  
25  
26  
27  
28  
29  
30  
31  
32  
33  
34  
35  
36  
37  
38  
39  
40  
41  
42  
43  
44  
45  
46  
47  
48  
49  
50  
51  
52  
53  
54  
55  
56  
57  
58  
59  
60  
61  
62  
63  
64  
65



**Fig. 6.** Pressure profile of coolant.

1  
2  
3  
4  
5  
6  
7  
8  
9  
10  
11  
12  
13  
14  
15  
16  
17  
18  
19  
20  
21  
22  
23  
24  
25  
26  
27  
28  
29  
30  
31  
32  
33  
34  
35  
36  
37  
38  
39  
40  
41  
42  
43  
44  
45  
46  
47  
48  
49  
50  
51  
52  
53  
54  
55  
56  
57  
58  
59  
60  
61  
62  
63  
64  
65



1  
2  
3  
4  
5  
6  
7  
8  
9  
10  
11  
12  
13  
14  
15  
16  
17  
18  
19  
20  
21  
22  
23  
24  
25  
26  
27  
28  
29  
30  
31  
32  
33  
34  
35  
36  
37  
38  
39  
40  
41  
42  
43  
44  
45  
46  
47  
48  
49  
50  
51  
52  
53  
54  
55  
56  
57  
58  
59  
60  
61  
62  
63  
64  
65

**Fig. 7.** Flowchart of the coupling system for burnup calculation during steady state condition.



**Fig. 8.** Bushehr NPP core modeled in MCNPX.

DESCRIPTION OF THE FIGS,

COLOR SUEING ETC ?

1  
2  
3  
4  
5  
6  
7  
8  
9  
10  
11  
12  
13  
14  
15  
16  
17  
18  
19  
20  
21  
22  
23  
24  
25  
26  
27  
28  
29  
30  
31  
32  
33  
34  
35  
36  
37  
38  
39  
40  
41  
42  
43  
44  
45  
46  
47  
48  
49  
50  
51  
52  
53  
54  
55  
56  
57  
58  
59  
60  
61  
62  
63  
64  
65

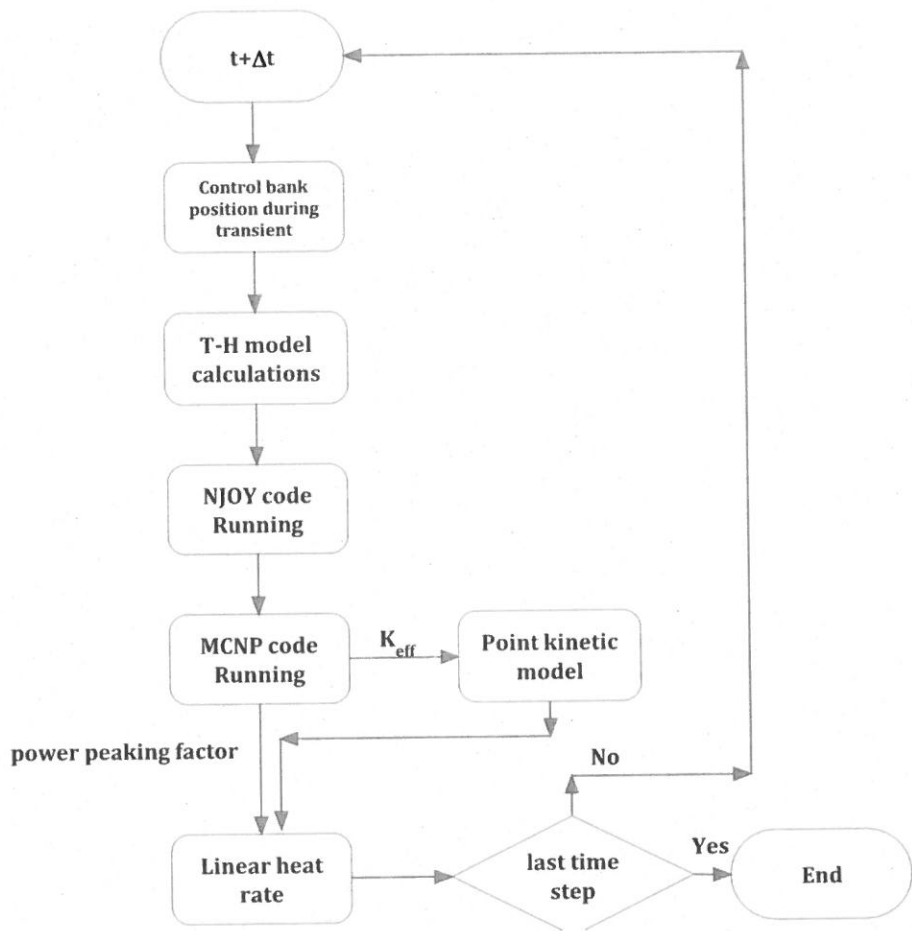


**Fig. 9.** Flowchart of coupling system during transient calculation.

WHAT IS FSAR?

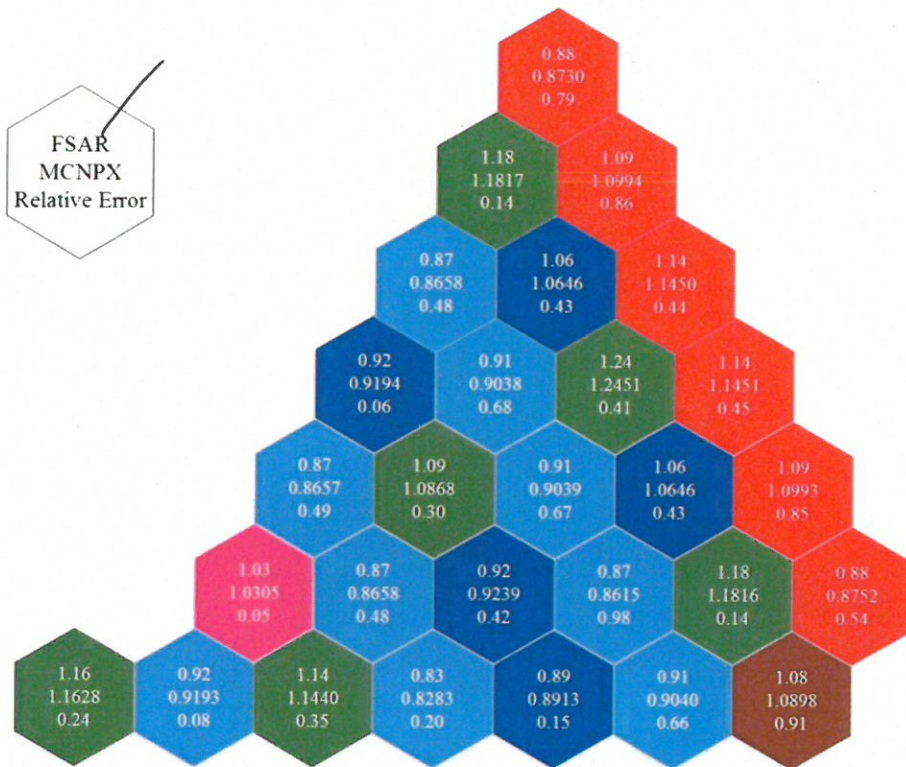
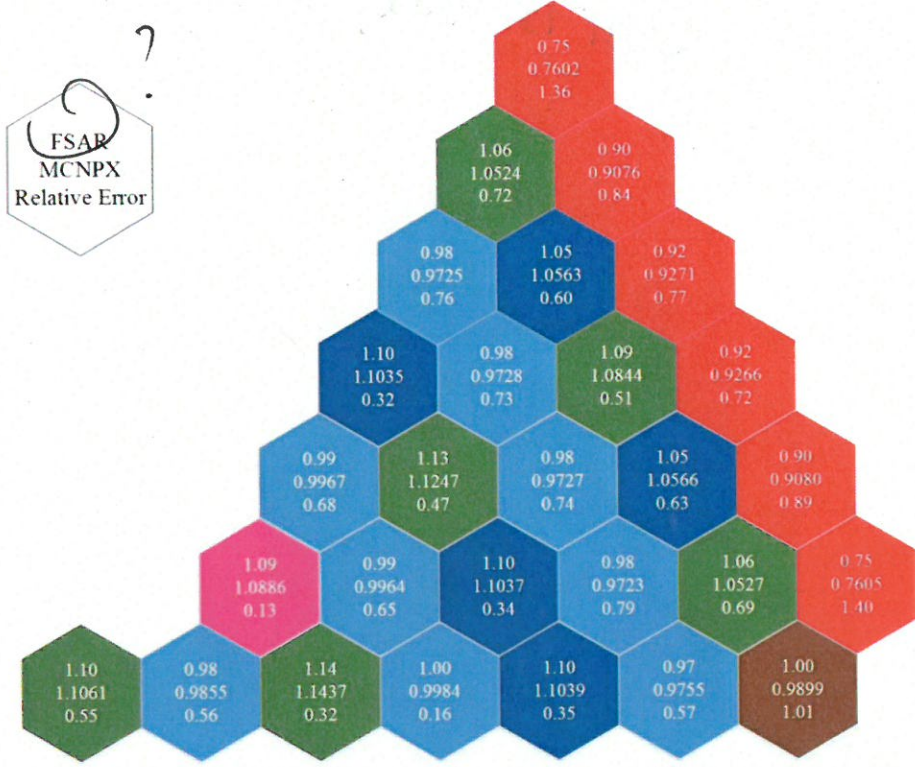
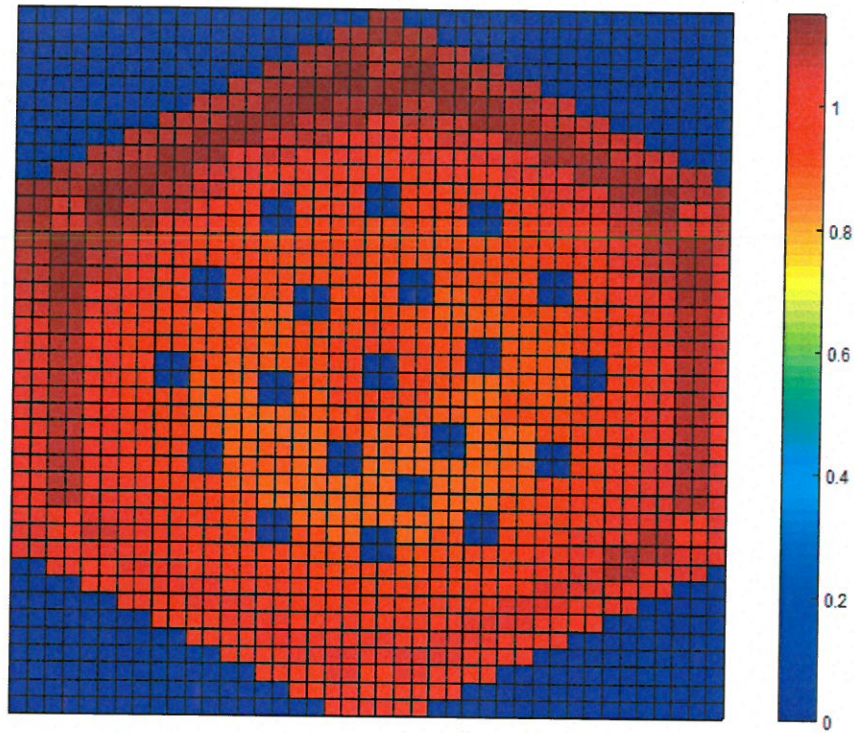


Fig. 10. Comparison between values of radial PPF in the beginning of cycle.

?  
POWER PEAK FACTOR?



**Fig. 11.** Comparison between values of radial PPF in the end of cycle.



**Fig. 12.** Fuel rod PPF( $K_r$ ) in the fuel assembly that most-powered fuel rod placed in the  
BOC.

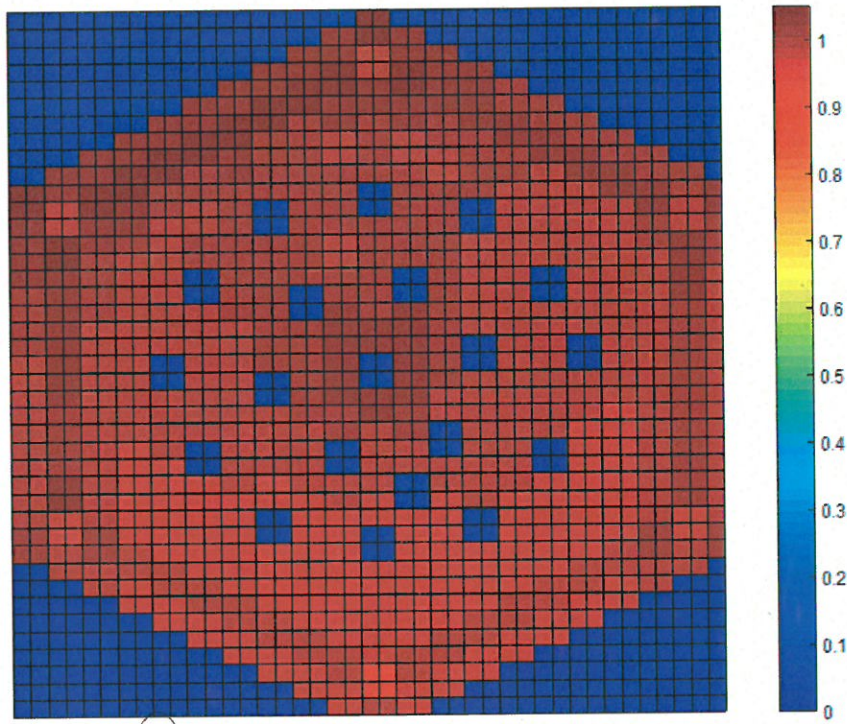


Fig. 13. Fuel rod PPF ( $K_r$ ) in the fuel assembly that most-powered fuel rod placed in the EOC.

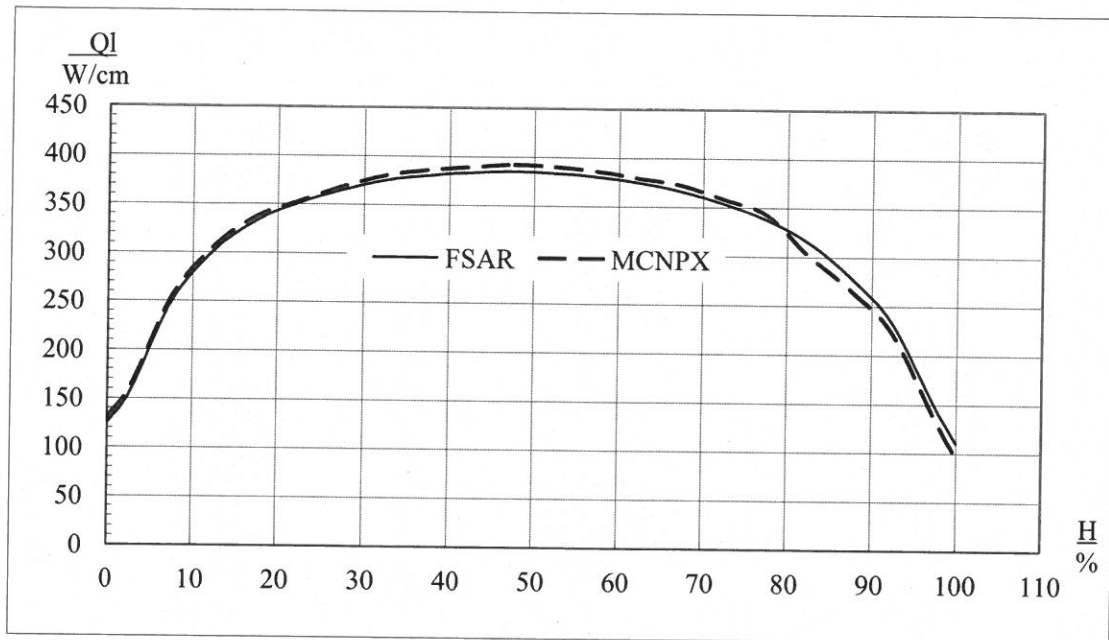


Fig. 14. Axial linear heat rate profile in steady state condition for the BOC.

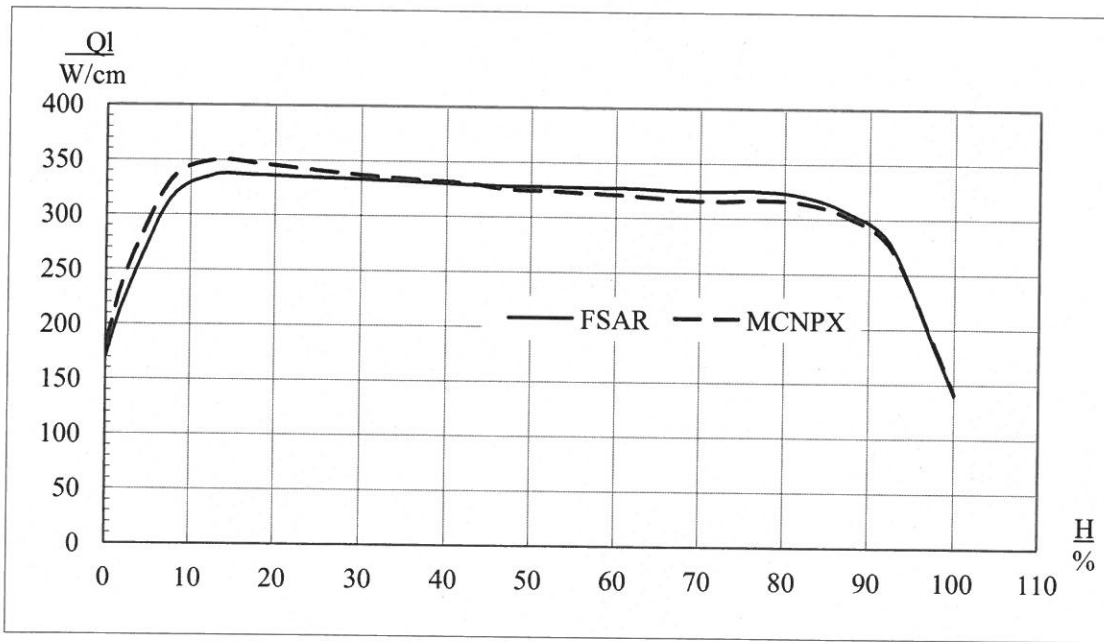


Fig. 15. Axial linear heat rate profile in steady state condition for the EOC.

(CAPTIONS OF FIGS 14-15  
NEED TO BE LARGELY IMPROVED  
TO CLARIFY THE DIFFS BETWEEN THEM)

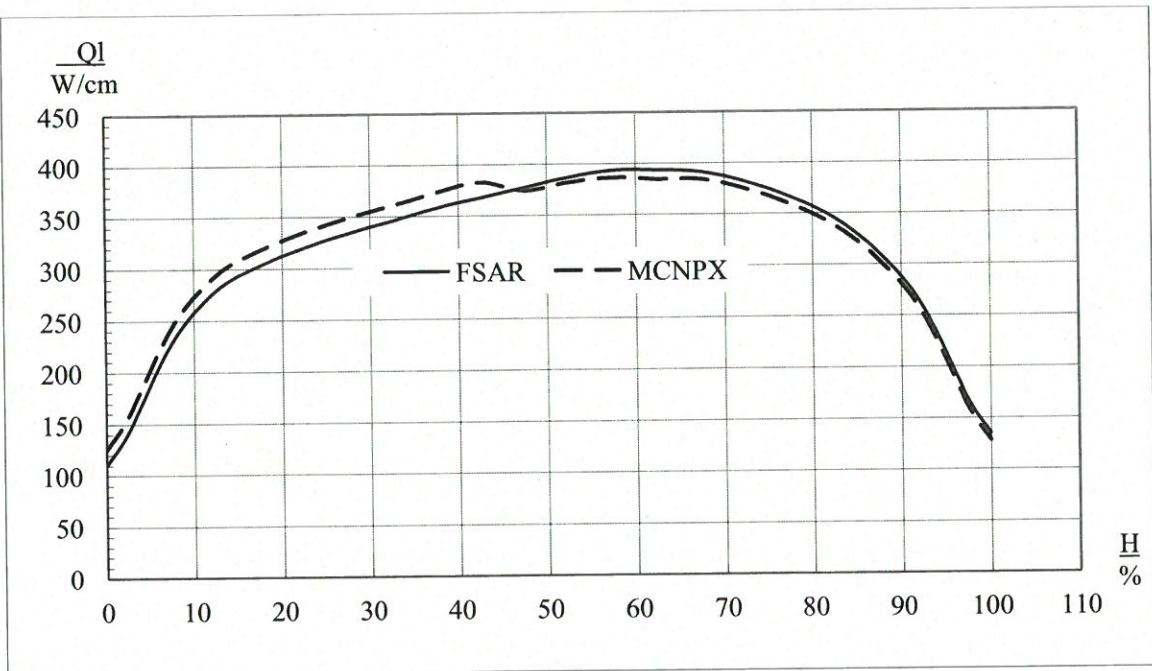


Fig. 16. Axial linear heat rate profile in initial condition for the BOC.

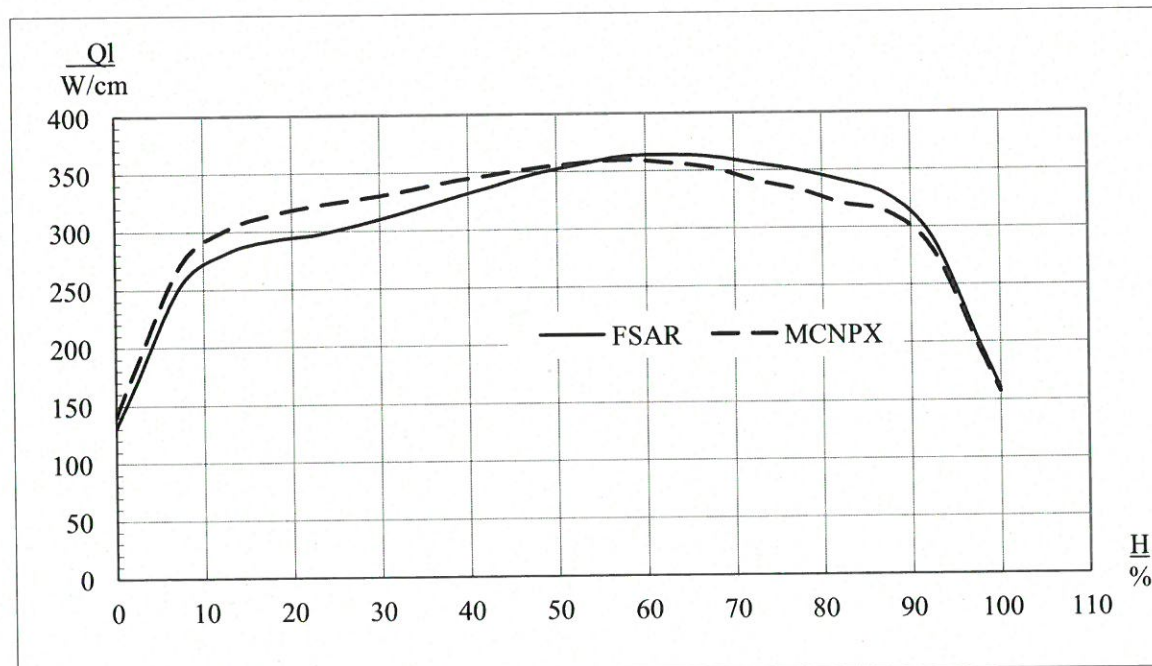


Fig. 17. Axial linear heat rate profile in initial condition for the EOC.

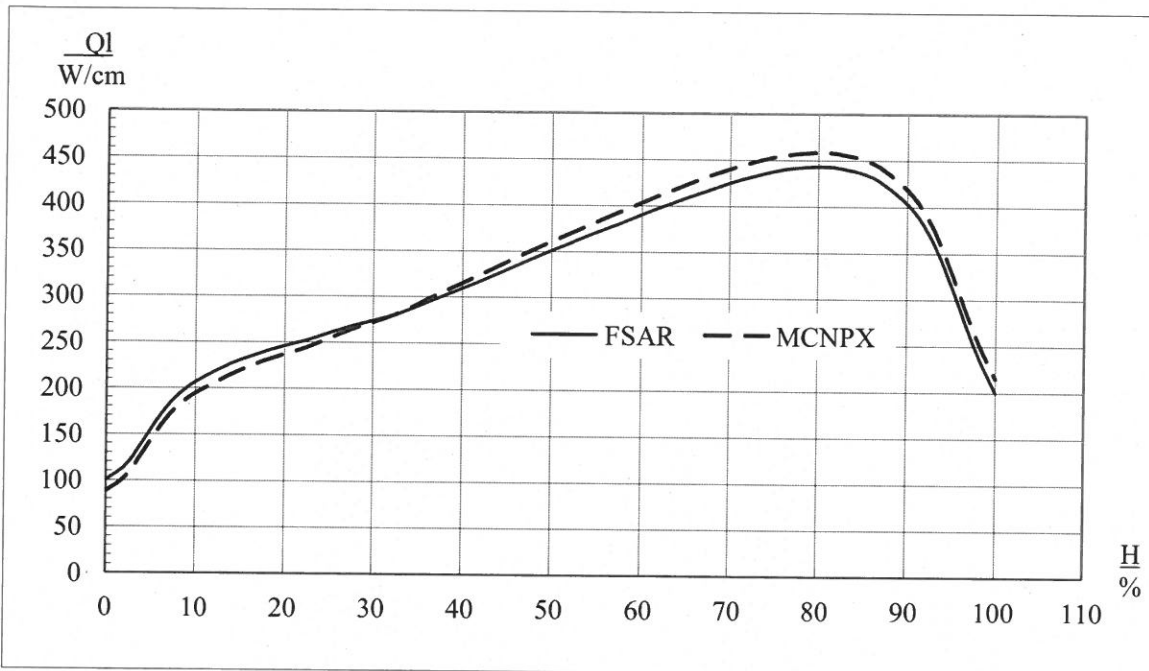


Fig. 18. Axial linear heat rate profile in final condition for the BOC.

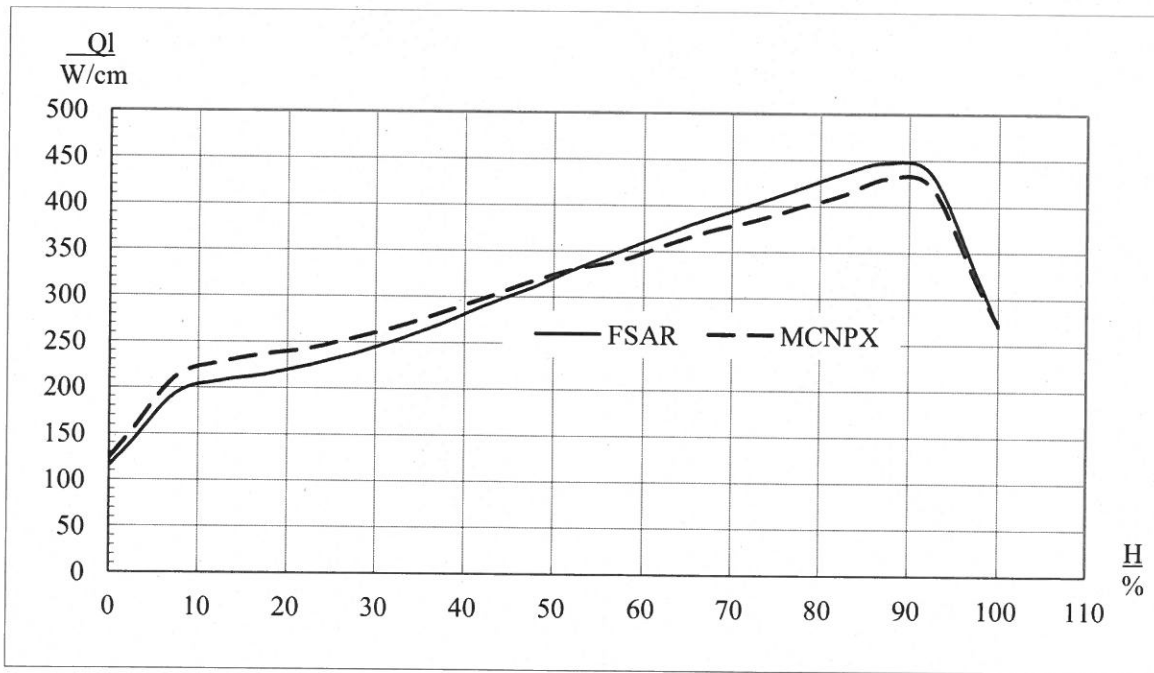


Fig. 19. Axial linear heat rate profile in final condition for the EOC.

## **\*Abstract**

### **ABSTRACT**

Error in movement of control rods that leads to Error in suppression of xenon oscillations refer to anticipated operational occurrences. Errors related to this occurrence could be treated as a long-term absence of some special actions used to stabilize the power field or incorrect movements of the control and protection system absorber rod. In this study, the movement of control rod, causing maximum power tilt, has been simulated in a WWER-1000 reactor by using coupling system contains Monte Carlo method for neutronic calculations, a single heated channel model for thermal hydraulic calculations and point kinetic model that all of these components are externally coupled by MATLAB system. The results of developed single heated channel model have been checked with RELAP5 results for WWER-1000. Analyses are based on linear heat rate of the most-powered fuel rod according to the WWER-1000 final safety analysis report. First, we determined the position of this most-powered fuel rod at desired cycle time steps by our developed coupling system. Then the most-powered fuel rod is segmented axially into equally spaced zones to study the effect of axial linear heat rate profile during desired transient. Finally, the results have been compared with Final Safety Analysis Report of WWER-1000 reactor. It is seen that there is a proper similarity between calculated and reported results.